Synthesis and Magnetic Properties of Mesostructured γ-Fe_2O_3/Carbon Composites by a Co-casting Method

Xiaoping Dong, Hangrong Chen, Wenru Zhao, Xia Li, and Jianlin Shi*

State Key Laboratory of High Performance Ceramics and Superfine Microstructures, Shanghai Institute of Ceramics, Chinese Academy of Sciences, 1295 Ding-xi Road, Shanghai 200050, P. R. China

Received April 2, 2007. Revised Manuscript Received May 9, 2007

A new co-casting method has been developed to synthesize novel mesostructured γ-Fe_2O_3/C composites with γ-Fe_2O_3 nanoparticles embedded in the wall of ordered mesoporous carbon materials. Fe^{3+} ions were captured by the framework of polyfurfuryl alcohol in the channel of mesoporous silica; during the carbonization process, $FeCl_3 \cdot 6H_2O$ was decomposed and magnetic γ-Fe_2O_3 nanoparticles were formed and confined in the carbon framework. The γ-Fe_2O_3/C composite materials were characterized using X-ray diffraction (XRD), nitrogen sorption, Mössbauer spectroscopy, X-ray photoelectron spectroscopy (XPS), transmission electron microscopy (TEM), and energy-dispersive X-ray (EDX) spectroscopy techniques; the magnetization strength was measured on a vibrating-sample magnetometer (VSM). Different amounts of magnetic iron oxides could be introduced into the composites, which led to varied specific saturation magnetizations. Near-zero coercivity and remanance indicate the superparamagnetic behavior of the composites.

Introduction

Ordered siliceous mesoporous materials have attracted considerable attention since they were first reported for the potential applications in heterogeneous catalysis, host−guest chemistry, environmental technology, adsorption, chemical sensors, and electrodes because of their large specific surface area, uniform pore size distribution, high thermal stability, and surface properties.[1−4] From the viewpoint of applications, the design and synthesis of nonsiliceous mesoporous materials are even more important than siliceous materials. However, their syntheses are much more difficult if compared with that of siliceous materials. It is hard to precisely control the hydrolysis and polymerization process of the nonsiliceous precursor, which causes poorly ordered porous structure.[5] Additionally, the amorphous pore wall of most mesoporous materials using surfactant template would limit their applications in many fields because of the poor thermal and mechanical stability. As an effective and promising strategy, nanocasting routes have been developed in recent years. It provides a pathway to prepare novel mesostructured materials with different framework compositions. Generally, the siliceous mesoporous material is used as the hard template, and inorganic or organic precursors are introduced to fill the void of pore channels. When the precursors are decomposed or polymerized, cross-linked nonsiliceous nanorods occupy the channels of the hard template. After removing the mold, a nonsiliceous negative replica to the hard template is obtained. So far, numerous novel nanostructure or nanoarrayed materials with this method have been reported.[6−8] Among them, ordered mesoporous carbon is no doubt the most successful one. Ryoo et al. first reported the synthesis of mesoporous carbon materials (CMK-1, 4) via a nanocasting route using mesoporous silica MCM-48 as a hard template. Since then, various types of mesoporous silica and carbon precursors have been adapted to synthesize mesoporous carbons, such as CMK-1 from MCM-48,[9] CMK-2 from SBA-1,[10] CMK-3 from SBA-15,[11] CMK-5 from SBA-15,[12] and so on. Unfortunately, when preparing mesostructured metal oxides, the metal precursors tend to deposit on the external surface of the mesoporous silica, which leads to large particles growing outside the channels. Thus, for filling the mesopores of templates, more precursors are needed, which would lead to an obvious reduction in surface area and pore volume. On the other hand, though mesoporous carbon is easy to prepare, it is also difficult to load functional nanoparticles into the mesopores because of its open pore structure in between the carbon nanorods and the hydrophobic nature of carbon surface.

Nanoscale magnetic particles have attracted many interests due to their widely promising applications, such as protein and enzyme immobilization, RNA and DNA purification,

* Corresponding author. Tel: 86-21-52412714. Fax: 86-21-52413122. E-mail: jlshi@sunm.shcnc.ac.cn.

(1) Corma, A. *Chem. Rev.* **1997**, *97*, 2373.
(2) Ciesla, U.; Schuth, F. *Microporous Mesoporous Mater.* **1999**, *27*, 131.
(3) Ying, J. Y.; Mehnert, C. P.; Wong, M. S. *Angew. Chem., Int. Ed.* **1999**, *38*, 56.
(4) Davis, M. E. *Nature* **2002**, *417*, 813.
(5) Lu, A-H.; Schuth, F. *Adv. Mater.* **2006**, *18*, 1793.
(6) Shin, H. J.; Ryoo, R.; Liu, Z.; Erasaki, T. O. *J. Am. Chem. Soc.* **2001**, *123*, 153.
(7) Lee, K.; Kim, Y.; Han, S. B.; Kang, H.; Park, S.; Seo, W. S.; Park, J. T.; Kim, P.; Chang, S. *J. Am. Chem. Soc.* **2003**, *125*, 6844.
(8) Tian, B.; Liu, X.; Yang, H.; Xie, S.; Yu, C.; Tu, B.; Zhao, D. *Adv. Mater.* **2003**, *15*, 1370.
(9) Ryoo, R.; Joo, S. H.; Jun, S. *J. Phys. Chem. B* **1999**, *103*, 7743.
(10) Ryoo, R.; Joo, S. H.; Jun, S.; Tsubakiyama, T.; Terasaki, O. *Stud. Surf. Sci. Catal.* **2001**, *135*, 150.
(11) Jun, S.; Joo, S. H.; Ryoo, R.; Kruk, M.; Jaroniec, M.; Liu, Z.; hsuna, T. O.; Terasaki, O. *J. Am. Chem. Soc.* **2000**, *122*, 10712.
(12) Joo, S. H.; Choi, S. J.; Oh, I.; Kwak, J.; Liu, Z.; Terasaki, O.; Ryoo, R. *Nature* **2001**, *42*, 169.

10.1021/cm0709065 CCC: $37.00
Published on Web 06/13/2007

separation of biochemical products and catalysts, and targeted drug delivery.[13,14] For the above applications, magnetic particles need to be well-dispersed and chemically stable. So, magnetic carrier technologies in which magnetic particles are incorporated into organic or inorganic matrixes become promising. Ordered mesoporous materials as inorganic carriers have been studied, which not only ensures the stabilization of magnetic particles and avoids their aggregation but also enables their size control and their organization in one-, two- and three-dimensional arrays.[15] However, it also has its drawbacks. The incorporated nanoparticle in the channel will cause the remarkable reduction of pore volume and surface area, and the pore blockage, which would obstruct the mass transfer. In addition, as limited by the pore dimension, the magnetic particles within the pore channels usually show rather low magnetization strength. In our previous work, a novel kind of magnetic core/mesoporous silica shell nanospheres with a uniform particle size was synthesized, which exhibits promising application for targeted drug delivery in the future.[16] However, high coercivity and remanance limit its biologic applications, as superparamagnetic behavior is preferred for these applications.[17] Mesoporous carbon used as the magnetic carrier is promising because of its open porous structure; however, the large size of magnetic particle would reduce the surface area when the guest concentration rises.[18−20]

Herein, we present a novel co-casting route to prepare mesostructured magnetic γ-Fe_2O_3/C composites with high γ-Fe_2O_3 content, large surface area, pore volume and uniform pore size. Carbon is the main composition of the framework, and magnetic nanoparticles or nanorods are embedded in the carbon walls with no large γ-Fe_2O_3aggregations found outside of the composites. The composite shows a superparamagnetic behavior with reasonably high magnetization strength.

Experimental Section

The mesoporous silica template SBA-15 was prepared according to the literature.[21] In a typical preparation, the starting composition was 4.0 g of Pluronic P123, 8.5 g of tetraethylorthosilicate (TEOS), 120 g of HCl (2M) and 30 g of H_2O. After the reaction at 313 K for 24 h, the mixture was then transferred into autoclaves and hydrothermally treated at 373 K for 2 days. The solid product was filtered, washed with distilled water, dried at 343 K, and calcined in air at 773 K (1 K/min) for 4 h.

The magnetic γ-Fe_2O_3/C composites were synthesized using SBA-15 as the hard template, $FeCl_3 \cdot 6H_2O$ as iron source, and furfuryl alcohol as carbon source. Typically, 1.5 mL of furfuryl alcohol and a small quantity of oxalic acid were dissolved in 10 mL of alcohol. This solution was incorporated into 1 g of SBA-15 by the wetness impregnation technique. After evaporating the ethanol and polymerizing furfuryl alcohol at 363 K, the residual unpolymerized furfuryl alcohol was evaporated at 423 K. The iron source was introduced into the composite via the wetness impregnation technique. Certain mass $FeCl_3 \cdot 6H_2O$ was dissolved in 10 mL of ethanol, and this solution was then mixed with the polyfurfuryl alcohol/SiO_2 composite. Being evaporated off the ethanol, the composite was thermal-treated in argon at 873 K to carbonize the polyfurfuryl alcohol. The silica template in the composite was removed by twice washing with heated 2 M NaOH solution. The template-free mesoporous γ-Fe_2O_3/C array was collected by filtering, washed with water and ethanol, and dried at 333 K; this sample is denated as meso-Fe/C. A reference sample with 5 wt % iron oxide content, Fe/meso-C, was prepared via loading $FeCl_3$ into a template-free mesoporous carbon under the same condition as that for meso-Fe/C.

Powder X-ray diffraction (XRD) patterns were recorded on a Rigaku D/MAX-2250V diffractometer using Cu−Kα radiation (40 kV and 40 mA). The scanning rate was 0.6°/min and 8°/min for the low-angle and high-angle XRD measurements, respectively. ^{57}Fe Mössbauer spectrum were recorded on a Wissel spectrometer in the constant acceleration mode, using a ^{57}Co(Pd) source. X-ray photoelectron spectroscopy (XPS) analysis was carried out on a Vacuum Generators Microlab 310-F spectrometer equipped with Mg K (1253.6 eV) operating at 200 W. Pressure in the analysis chamber ranged from 1×10^{-8} to 1×10^{-9} mbar and low-intensity X-rays were focused on an area of about 40 mm^2 in size. Calibration of spectra was performed by taking the C 1s electron peak (BE = 284.6 eV) as internal reference. Nitrogen adsorption and desorption isotherms at 77 K were measured on a Micromeritics Tristar 3000 system. Before measurement, samples were pretreated at 473 K for 12 h under nitrogen. The specific surface areas and the pore size distributions were calculated from the BET and BJH data, respectively. Transmission electron microscopy (TEM) images were obtained on a JEOL 200CX electron microscope operated at 160 kV. Energy dispersive X-ray spectra (EDX) were collected from an attached Oxford Link ISIS energy-dispersive spectrometer fixed on a JEM-2010 electron microscope operated at 200 kV. A vibrating-sample magnetometer (VSM, Model BHF-55) was used to study the magnetic properties.

Results and Discussions

Figure 1 illustrates the schematic procedure used in the present work for the synthesis of mesostructured magnetic Fe_xO_y/C composites. In step 1, after removing the surfactant template from mesoporous silica by calcination, furfuryl alcohol was introduced into the channel and then polymerized under the catalysis by oxalic acid. Though the polymer has occupied the channel of mesoporous template, abundant small cavities still remained in the polymer framework, which make numerous Fe^{3+} ions be adsorbed in between (step 2). In step 3, polyfurfuryl alcohol was carbonized under N_2 at 873 K; meanwhile, $FeCl_3 \cdot 6H_2O$ was decomposed to oxide. The mesoporous silica template provides a confined space to the growth of iron oxide crystal only along the channel of mesoporous template. In addition, during the conversion of the cross-linked polymer web into compact carbon, the carbon also provides a block to confine the growth of iron

(13) Tong, X.-D.; Sun, Y. *Biotechnol. Prog.* **2001**, 738.
(14) Gruttner, C.; Rudershausen, S.; Teller, J. *J. Magn. Magn. Mater.* **2001**, *225*, 1.
(15) Matsura, V.; Guari, Y.; Larionova, J.; Guerin, C.; Caneschi, A.; Sangregorio, C.; Lancelle-Beltran, E.; Mehdi, A.; Corriu, R. J. P. *J. Mater. Chem.* **2004**, *14*, 3026.
(16) Zhao, W.; Gu, J.; Zhang, L.; Chen, H.; Shi, J. *J. Am. Chem. Soc.* **2005**, *127*, 8916.
(17) Wang, Z.; Guo, H.; Yu, Y.; He, N. *J. Magn. Magn. Mater.* **2006**, *302*, 397.
(18) Lu, A-H.; Schmidt, W.; Matoussevitch, N.; Bönnemann, H.; Spliethoff, B.; Tesche, B.; Bill, E.; Kiefer, W.; Schüth, F. *Angew. Chem., Int. Ed.* **2004**, *43*, 4305.
(19) Park, I.-S.; Choi, M.; Kim, T.-W.; Ryoo, R. *J. Mater. Chem.* **2006**, *16*, 3409.
(20) Lee, J.; Lee, D.; Oh, E.; Kim, J.; Kim, Y.-P.; Jim, S.; Kim, H.-S.; Hwang, Y.; Kwak, J. H.; Park, J.-G.; Shin, C.-H.; Hyeon, T. *Angew. Chem., Int. Ed.* **2005**, *44*, 7427.
(21) Zhao, D.; Feng, J.; Huo, Q.; Melosh, N.; Fredrickson, G. H.; Chmelka, B. F.; Stucky, G. D. *Science* **1998**, *279*, 548.

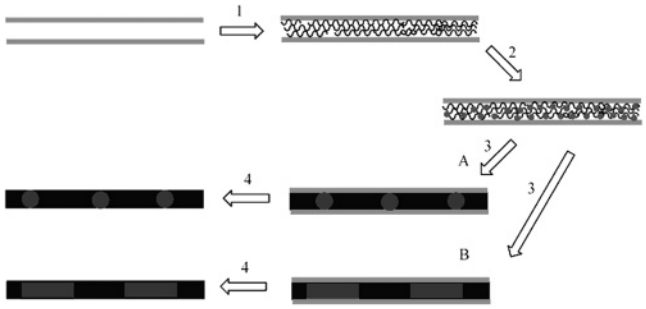

Figure 1. Schematic illustrations of preparing mesostructured meso-Fe/C composites: (1) the furfuryl alcohol introduction into the channel of mesoporous silicas and polymerization; (2) iron ion absorption by the polyfurfuryl alcohol framework; (3) carbonization of the polyfurfuryl alcohol and the precursor decomposition to oxides in nanoparticle form with low Fe precursor content (A) and in nanorod form with high Fe precursor content (B); (4) Removal of the silica template.

oxide. Such a double limitation makes iron oxide particles and/or nanorods grow only within the pore channels of the silica template, and they are finally embedded in the carbon framework. When the content of introduced Fe precursor is low, iron oxide nanoparticles form (A), and at increased amounts of the Fe precursor, iron oxide particles aggregate and grow into the nanorodlike form (B). After the silica template was removed by 2 M NaOH aqueous solution, mesostructured magnetic meso-Fe/C composites were obtained (step 4).

There are several previous reports on the preparation of functional mesoporous carbon via loading guest nanoparticles;[22−24] however, the guest particles commonly occupied the pore channels. In our recent work, a novel MnO_2 embedded in carbon structure was obtained by the direct reaction between the oxidant ($KMnO_4$) and the reductant (mesoporous carbon).[25] The amount of manganese can be controlled according to the reaction time and the concentration of $KMnO_4$ aqueous solution. However, a long reaction time for the purpose of high MnO_2 content loading would reduce the ordering of mesopores, and even result in pore structure collapsing in some areas because of the damage of the ordered carbon framework; therefore, the unconfined growth of MnO_2 particles can be found in the case of a high loading amount. In the present work, Fe^{3+} ions were introduced into the polymerized polyfurfuryl alcohol/silica template matrix, iron oxides formed but were not limited to grow only into nanoparticles and they could also further grow along and within the pore channels of the mesoporous silica into nanorods under the confinement by the hard silica template; therefore, the dimensions of either nanoparticles or nanorods are limited by the pore size of silica template. In this way, we can obtain magnetic mesostructured iron oxide/C composites with magnetic iron oxides present in quasi-zero-dimensional nanoparticle and/or one-dimensional nanorod forms. Comparatively, when $FeCl_3$ was loaded into a

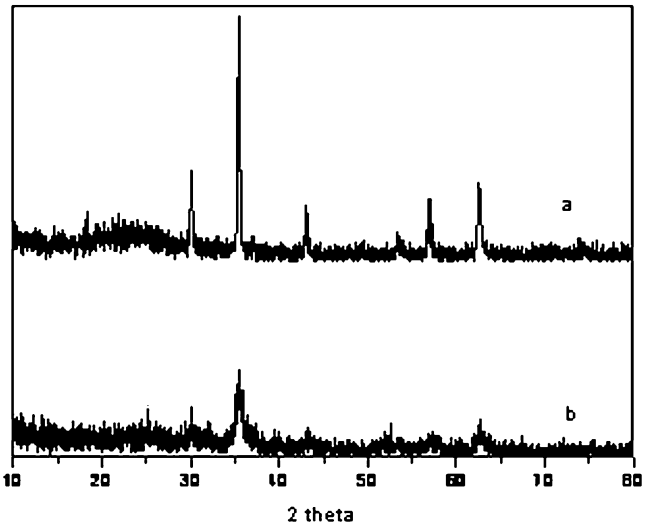

Figure 2. High-angle XRD pattern of (a) the reference sample and (b) mesostructured meso-Fe/C-20 composites.

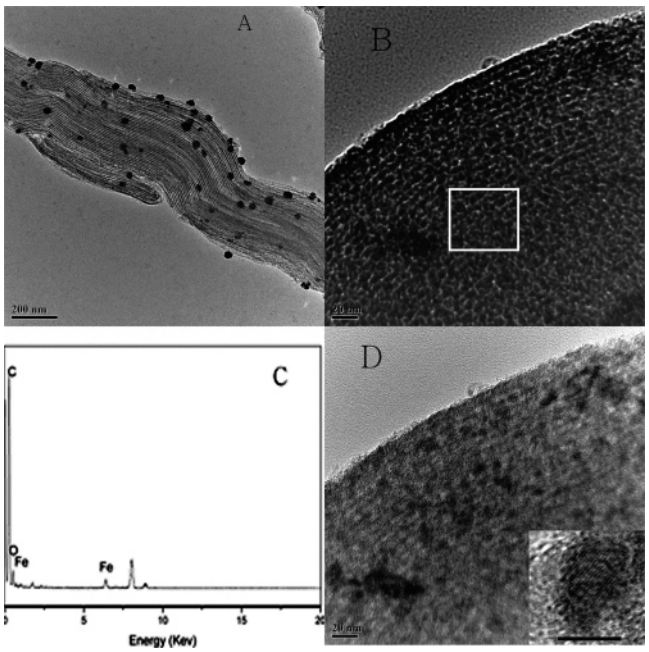

Figure 3. (A) TEM image of the reference sample; (B) TEM image of mesostructured meso-Fe/C-20 composites; (C) energy-dispersive X-ray (EDX) spectrum taken from the square area in B; (D) TEM image of mesostructured meso-Fe/C-20 composites taken at the same area as in B but under enhanced electron beam density, giving a much increased brightness; the inset in D is the HRTEM image of a γ-Fe_2O_3 nanoparticle (the scale bar is 5 nm).

template-removed mesoporous carbon (Fe/meso-C) under the same condition as that for meso-Fe/C composites, large iron oxide particles can be found growing outside of mesoporous carbon (Figure 3A). The high-angle XRD results are shown in Figure 2. Strong and sharp peaks of iron oxide are found in such a reference sample, indicating that large iron oxidecrystals formed outside of the carbon particles. In contrast, magnetic meso-Fe/C composites exhibit much weaker and broader characteristic diffraction peaks of iron oxide, illustrating that the nanoscale dimension of iron oxides as confined by the templates. The pattern of diffraction peaks is in accordance with that of either magnetite (Fe_3O_4) or maghemite (γ-Fe_2O_3), which all have magentism. Figure 3B is a TEM image of meso-Fe/C. The image shows that the

(22) Zhu, S.; Zhou, H.; Hibino, M.; Honma, I.; Ichihara, M. *Adv. Funct. Mater.* **2005**, *15*, 381.
(23) Joo, S. H.; Choi, S. J.; Oh, I.; Kwak, J.; Liu, Z.; Terasaki, O.; Ryoo, R. *Nature* **2001**, *412*, 169.
(24) Grigoriants, I.; Sominski, L.; Li, H.; Ifargan, I.; Aurbach, D.; Gedanken, A. *Chem. Commun.* **2005**, 921.
(25) Dong, X.; Shen, W.; Gu, J.; Xiong, L.; Zhu, Y.; Li, H.; Shi, J. *Micropor. Mesopor. Mater.* **2006**, *91*, 120.

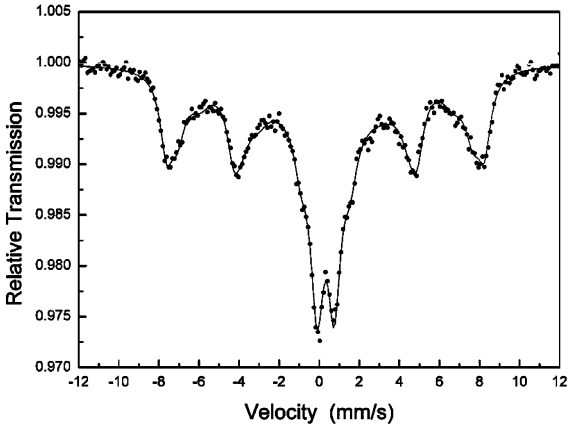

Figure 4. RT Mössbauer spectrum of meso-Fe/C-20 sample.

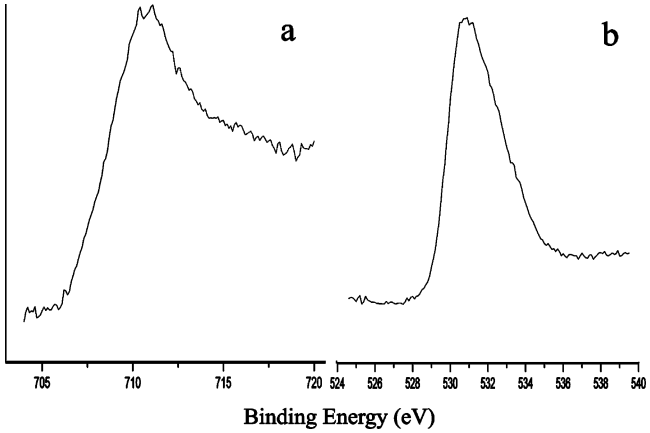

Figure 5. XPS spectra of meso-Fe/C-20 sample for (a) $Fe2p_{3/2}$ and (b) O1s.

ordered structure of meso-Fe/C composites, an exact negative replica of SBA-15 with a hexagonal arrangement of cylindrical mesoporous tubes, has been preserved. A uniform pore size of about 3−4 nm can be observed, which is in accordance with the wall thickness of SBA-15. No bulk aggregates of iron oxides can be found outside of the mesoporous carbon particle, and also no nanoparticles larger size than the wall thickness of the composites can be found. The much darker areas in the region of meso-Fe/C composite framework are believed to be iron oxide nanoparticles and/or nanorods because of their much higher density than carbon. The energy-dispersive X-ray (EDX) spectrum (Figure 3C) taken on the square area in Figure 3B gives the proof for the existence of Fe, O, and C. To reveal the existing state of magnetic iron oxide nanoparticles or nanorods in this composite, a much brighter image at the same area has been taken on the TEM under enhanced electron beam density, as illustrated in Figure 3D. In this image, carbon framework become bright enough so that pore channels and the low-density carbon framework can no longer be differentiated as clearly as in Figure 3B because of the high image brightness. However, the dark iron oxide nanoparticles are more clearly revealed, which are dispersed along the wall of carbon with uniform sizes corresponding to the pore diameters of the hard template. Magnetic nanoparticles may also show different brightness and/or contrast to the carbon framework due to the different particle sizes. The HRTEM image in the inset of Figure 3D illustrates a crystalline iron oxide nanoparticle of about 5 nm embedded in the wall of carbon in meso-Fe/C composites. Compared to the reference sample where large iron oxide particles are supported on the outside surface of template-removed mesoporous carbon, it can be concluded that using hard mesoporous silica templates is a key to preparing mesostructured meso-Fe/C composites when nanoscale iron oxide particles and/or nanorods are embedded within the carbon framework.

The RT Mössbauer spectrum of meso-Fe/C sample is shown in Figure 4. The spectrum can be fitted by a broad sextet and a doublet. The broad sextet indicates a wide distribution of iron oxide particle size,[26] which is due to the unlimited growth of the particles in the direction of pore channel. The strong doublet provides evidence that relatively large amount of superparamagnetic materials and/or paramagnetic Fe^{3+} exists in the meso-Fe/C composite. As we know, two sextets exist in the Mössbauer spectrum of Fe_3O_4, one corresponding to the tetrahedral site Fe^{3+} ion and the other to an average oxidation state of $Fe^{2.5+}$ ion in the octahedral site.[27] The absence of these two sextets illustrates the non-presence of Fe_3O_4, which implies that iron oxide exists in γ-Fe_2O_3 form if consulted with the result of XRD. Actually, we can also distinguish among γ-Fe_2O_3, α-Fe_2O_3, and Fe_3O_4 from the parameters in the Mössbauer spectrum. The value of isomer shift (IS) is 0.39 mm/s and hyperfine field (H) is 514 KOe for α-Fe_2O_3. In the case of Fe_3O_4, the IS and H values responding to the latter sextet are 0.75 mm/s and 453 KOe, respectively. Here, the Mössbauer parameters obtained from the spectrum are IS = 0.33 mm/s and H = 492 KOe, which are the typical values for γ-Fe_2O_3. However, the IS values of γ-Fe_2O_3 and α-Fe_2O_3 are identical within experimental error, and the α-Fe_2O_3 hyperfine magnetic field (H) can be diminished in very small particles by the effect of magnetic collective excitations.[28] So the quadrupole shift (QS) values become an effective parameter to distinguish between α-Fe_2O_3 and γ-Fe_2O_3. The 0 mm/s quadrupole shift value in our sample is in accordance with the reported one, which proves the γ-Fe_2O_3 form (the QS value of α-Fe_2O_3 is −0.22 mm/s).

From the XRD patterns, we cannot clearly distinguish between the γ-Fe_2O_3 and Fe_3O_4 phases; however, with the XPS technology it is easy to prove the valence of iron ions and thus to identify γ-Fe_2O_3 from Fe_3O_4. Magnetite contains both Fe^{2+} and Fe^{3+}, both of which contribute to the $Fe2p_{3/2}$ spectrum with the two overlapping components.[29] In total, the main peak of Fe_3O_4 for $Fe2p_{3/2}$ is 710.4 eV, slightly lower than that of Fe_2O_3, 710.7 eV.[30] Obviously, there is no Fe_3O_4 phase in our case (Figure 5a). A split was found in the main peak, which is proof to differentiate γ-Fe_2O_3 from α-Fe_2O_3.[29] The O1s spectrum is shown in Figure 5b. The peak is not

(26) Ni, Y.; Ge, X.; Zhang, Z.; Ye, Q. *Chem. Mater.* **2002**, *14*, 1048.

(27) Jiao, F.; Jumas, J.-C.; Womes, M.; Chadwick, A. V.; Harrison, A.; Bruce, P. G. *J. Am. Chem. Soc.* **2006**, *128*, 12905.

(28) Mørup, H.; Topsøe, S. *Appl. Phys.* **1976**, *11*, 63.

(29) Briggs, D.; Seah, M. P. *Practical Surface Analysis*, 2nd ed.; Wiley InterScience: Hoboken, NJ, 1990 ; Vol. 1: Auger and X-ray Photoelectron Spectroscopy.

(30) Fujii, T.; de Groot, F. M. F.; Sawatzky, G. A.; Voogt, F. C.; Hibma, T.; Okada, K. *Phys. Rev. B* **1999**, *59*, 3195−3202.

Table 1. γ-Fe_2O_3 Contents and Pore Structure Parameters of meso-Fe/C Composites

sample	γ-Fe_2O_3 content (wt %)	BET surface area (m^2/g)	pore volume (cm^3/g)	pore size (nm)
meso-Fe/C-0	0	1357	1.56	3.4
meso-Fe/C-5	14.1	1243	1.54	3.8
meso-Fe/C-10	28.9	975	1.08	3.9
meso-Fe/C-20	55.4	599	0.59	3.6

so symmetric because of the existence of oxygen-containing groups (oxygen impurity) in a carbon framework. The reported values of O1s binding energy for α-Fe_2O_3 and Fe_3O_4 are identical (~530.0 eV), slightly lower than that for γ-Fe_2O_3 (530.6 eV).[30] The value of 530.8 eV obtained in the O1s spectrum matches well with γ-Fe_2O_3, and no shoulder peak is found at the lower binding energy side, indicating the absence of α-Fe_2O_3 and Fe_3O_4.

We also prepared the meso-Fe/C composites with different loading levels of iron oxide via adjusting the amount of $FeCl_3$, which was introduced into the polyfurfuryl alcohol/SiO_2 composite. These samples of different iron oxide contents are donated as meso-Fe/C-*x* ($x = 0, 5, 10, 20$), where *x* is the weight percent ratio of γ-Fe_2O_3 to polyfurfuryl alcohol/SiO_2 composite. The γ-Fe_2O_3 contents in the final products were estimated from the residue contents after calcining the composite materials in air at 873 K. The contents of γ-Fe_2O_3 in these samples are listed in Table 1.

These meso-Fe/C-*x* composite samples were characterized by XRD as shown in Figure 6. The meso-Fe/C-0 and meso-Fe/C-5 samples exhibit three well-resolved reflections in the 2θ range between 1 and 3°, which can be indexed as (100), (110), and (200) reflections associated with hexagonal symmetry (Figure 6A). Only one weak peak of (100) was detected in both the meso-Fe/C-10 and meso-Fe/C-20 samples in the low-angle range, which means that the ordered mesostructure has been destroyed after the content of iron oxide was destroyed. The high-angle XRD patterns of the meso-Fe/C-*x* composites in Figure 6B show broad γ-Fe_2O_3 characteristic diffraction peaks. The diffraction peaks in the meso-Fe/C-5 sample are very weak and broad, and these in meso-Fe/C-10 and meso-Fe/C-20 samples are much stronger and sharper, though they are still broad. This is due to the growth of γ-Fe_2O_3 nanoparticles into larger size and/or into nanorod form in the framework of carbon at increased γ-Fe_2O_3loading amount in meso-Fe/C composites.

Nitrogen sorption isotherms were recorded to investigate the effect of the γ-Fe_2O_3 content on the pore properties of the samples. Figure 7A shows the nitrogen sorption isotherms of meso-Fe/C-0, meso-Fe/C-5, meso-Fe/C-10, and meso-Fe/C-20 samples. All isotherm curves of the samples are found to be of type IV with a marked leap in the adsorption branch between relative pressures P/P_0 of 0.4 and 0.6, which is typical for mesoporous solids. This indicates that the ordered mesostructure of meso-Fe/C has been kept after the incorporation of γ-Fe_2O_3 nanoparticles or nanorods. The specific surface areas of these samples are obtained using the Brunauer−Emmett−Teller (BET) method, and the pore volume and pore size are calculated from the desorption branch using Barret−Joyner−Halenda (BJH) method. Large surface areas are retained after the incorperation of γ-Fe_2O_3

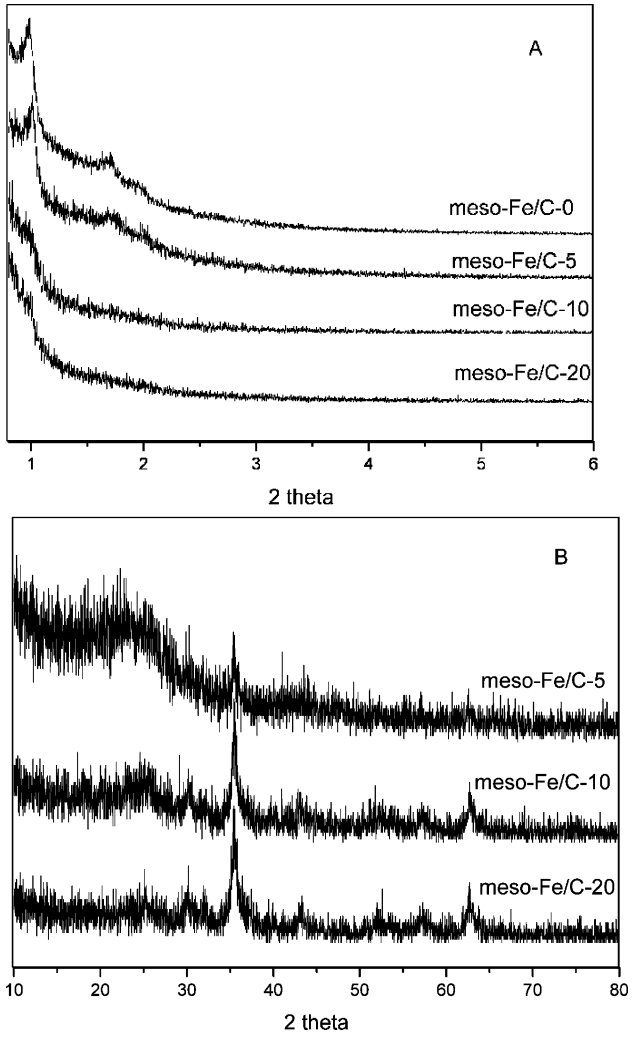

Figure 6. XRD patterns of mesostructured meso-Fe/C composites: (A) low-angle XRD patterns and (B) high-angle XRD patterns.

nanoparticles and/or nanorods, even at a γ-Fe_2O_3 content of 55.4 wt %. The surface area (Table 1) is found to decrease gradually from meso-Fe/C-0 to meso-Fe/C-20, and similarly, the pore volume decreases also in this order. The main reason for such decreases can be attributed to the presence of a large amount of γ-Fe_2O_3 because of its much higher density than carbon. However, similar pore size distributions for all meso-Fe/C composites, in a range of 3−4 nm, can be found in Figure 7B and Table 1. These data are the additional evidence for the γ-Fe_2O_3 nanoparticles (nanorods) embedded in carbon framework structure; otherwise, the presence of a high amount of iron oxide in pore channels must have led to the remarkable decrease of the pore size and much more severe reduction of surface area and pore volume according to the previous reports.[31−33] This result is in accordance with the TEM image of the composite.

Representative TEM images of the meso-Fe/C composites with different γ-Fe_2O_3 contents are shown in Figure 8 (some

(31) Zhang, W.; Shi, J.; Chen, H.; Hua, Z.; Yan, D. *Chem. Mater.* **2001**, *13*, 648.
(32) Zhang, L.; Shi, J.; Yu, J.; Hua, Z.; Zhao, X.; Ruan, M. *Adv. Mater.* **2002**, *14*, 1510.
(33) Li, L.; Shi, J.; Zhang, L.; Xiong, L.; Yan, J. *Adv. Mater.* **2004**, *16*, 1079.

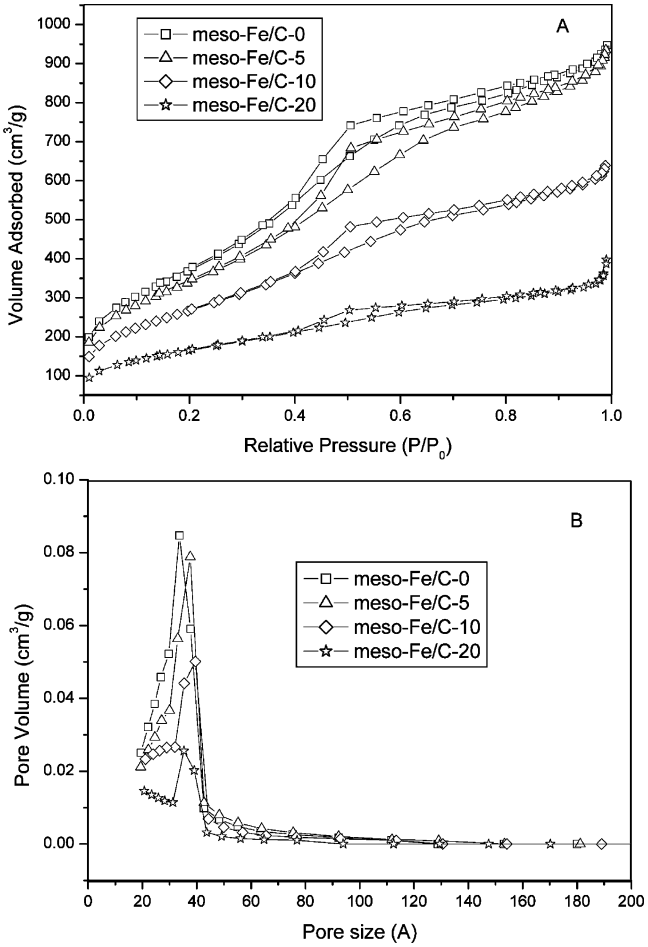

Figure 7. (A) Nitrogen sorption isotherms and (B) the corresponding pore size distribution for mesostructured meso-Fe/C composites

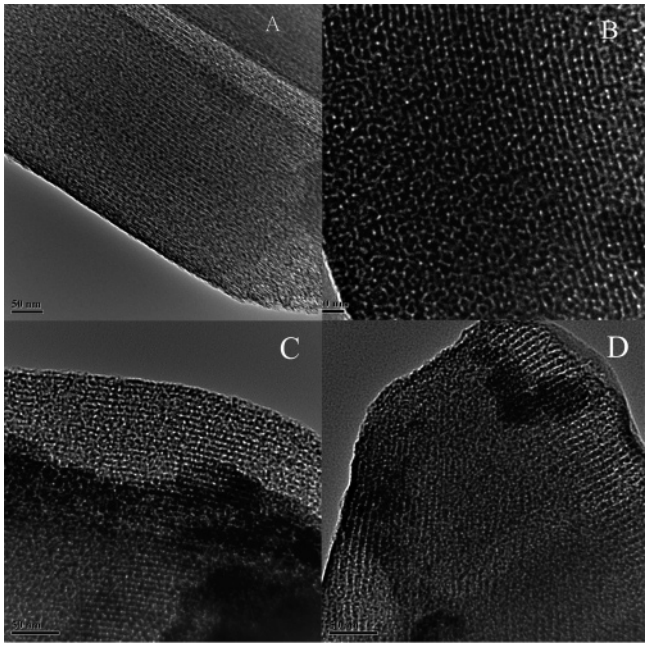

Figure 8. TEM images of mesostructured meso-Fe/C composites: (A) meso-Fe/C-0; (B) meso-Fe/C-5; (C) meso-Fe/C-10; (D) meso-Fe/C-20. The much blacker areas in C and D should be caused by the different thicknesses and/or the fragment attachment of the samples.

much blacker areas in C and D should be caused by the different thickness and/or the fragment attachment of the samples). For sample meso-Fe/C-0, only regular mesoporous

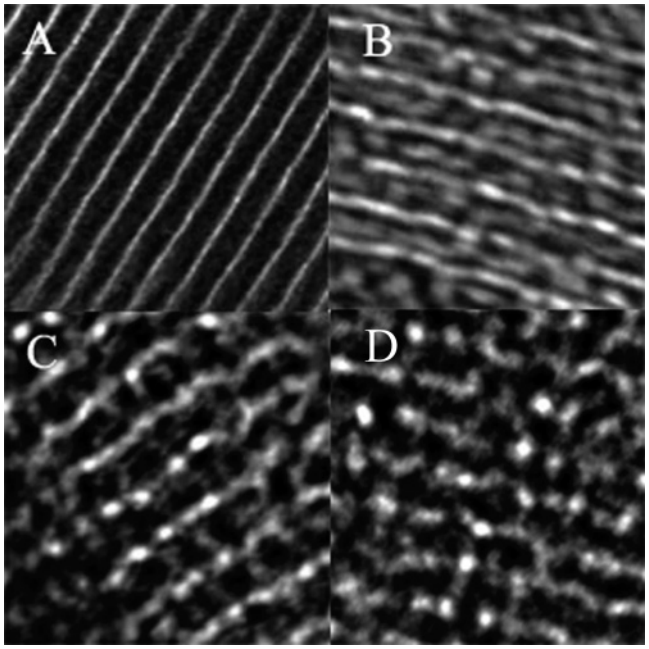

Figure 9. Magnified TEM images of (A) mesoporous carbon carbonized at 1173 K; (B) meso-Fe/C-0; (C) meso-Fe/C-5; (D) meso-Fe/C-10 carbonized at 873 K.

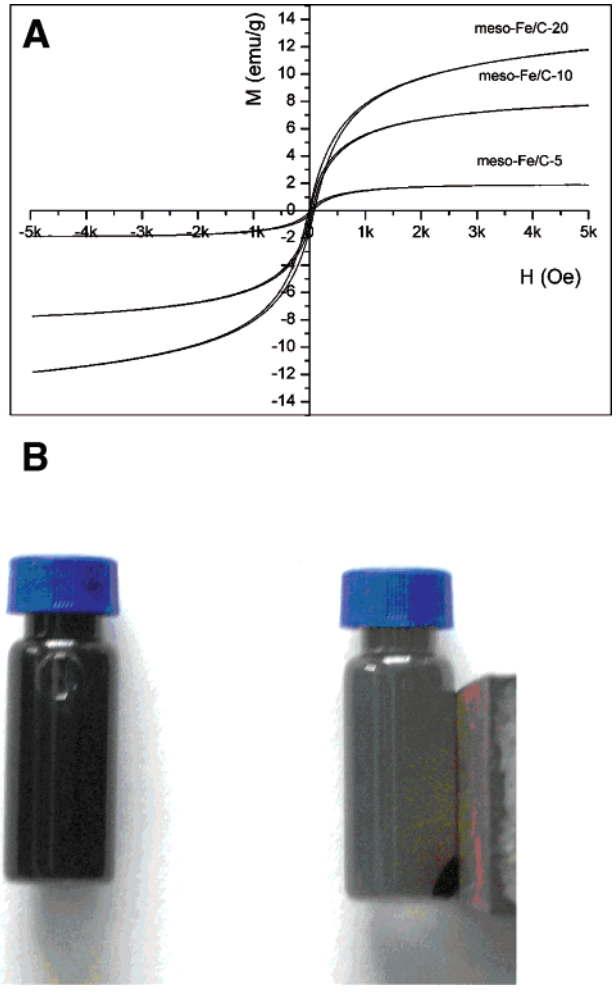

Figure 10. (A) magnetization curves of the meso-Fe/C-5, meso-Fe/C-10, and meso-Fe/C-20; (B) photograph of dispersed mesostructured meso-Fe/C in ethanol before (left) and after (right) being attracted by an outer magnet.

channels with hexagonal structure are identified. When the content of iron oxide increases, the ordered structure can

still be observed, even in the images of meso-Fe/C-10 and meso-Fe/C-20 samples, which exhibit very illegible small-angle XRD peaks (Figure 6A). From the magnified image (Figure 9), a rodlike carbon wall can be clearly identified in pure mesoporous carbon after carbonization at 1173 K, and the surface of the carbon wall is smooth. In the meso-Fe/C-0 sample, which was carbonized at a relatively low temperature of 873 K, a slightly rough surface is found; meanwhile, lots of lacunas are found in the carbon wall, due to the incomplete carbonization and the loose compaction, which led to lower XRD peak intensities than those of mesoporous carbon prepared at a higher temperatures. Accompanying the increase of Fe content, the surface of the carbon wall became much rougher, which reduced the ordering of carbon framework, resulting in more scattered small-angle XRD patterns in high-Fe-content samples.

Figure 10A shows the magnetization curves of the meso-Fe/C-5, meso-Fe/C-10, and meso-Fe/C-20 at room temperature. The near-zero coercivity and remanance on the magnetization curves indicate that most particles are superparamagnetic in nature and the very small coercivity and remanance are mainly caused by a fraction of larger iron oxides, such as long nanorod. The corresponding saturation magnetizations strengths (M_s) are 1.9, 7.7, and 11.7 emu/g, respectively. These values are much lower than that of bulk γ-Fe_2O_3,[26] which is attributed to the nanosize of the γ-Fe_2O_3 particles and the presence of carbon. After deducting the carbon percentages, the saturation magnetizations strengths of γ-Fe_2O_3 are 13.5, 26.6, and 21.1 emu/g, respectively. The value of meso-Fe/C-5 is much lower than those of meso-Fe/C-10 and meso-Fe/C-20, because of its much smaller particle size and much more obvious superparamagnetic behavior.[34] The magnetic separability of such magnetic composites was tested in ethanol by placing a magnet beside the glass bottle (Figure 10B). Without an outer magnet, the magnetic composite can be dispersed in ethanol to form a dark and stable suspension (left bottle). However, in the right bottle, the black particles were attracted to the magnet within a short time. This will provide an easy and effective way to separate the magnetic composite from suspensions.

(34) Wang, Q.; Yang, H.; Shi, J.; Zou, G. *Mater. Res. Bull.* **2001**, *36*, 503.

Conclusion

A novel structure of γ-Fe_2O_3nanoparticles (nanorods) embedded in the framework of mesoporous carbon has been developed by a facial and new co-casting process. All the results indicate that, the introduced iron precursor, $FeCl_3 \cdot 6H_2O$, were decomposed and in-situ confined within the carbon framework, being present in a magnetic γ-Fe_2O_3 form. γ-Fe_2O_3 grow into nanoparticle and/or nanorodlike forms within and along the wall of carbon framework due to the confinement of mesoporous silica hard template. Different γ-Fe_2O_3 amounts up to as high as 55.4 wt % can be incorperated, whereas high surface areas are maintained and pore size kept almost unchanged as compared to pure mesoporous carbon, even at a very high γ-Fe_2O_3 loading amount. Most nanoscale γ-Fe_2O_3 particles or rods in the meso-Fe/C composites exhibit superparamagnetic property, with the saturation magnetization strength of 11.7 emu/g at the highest loading amount. The novel co-casting method provides a common path to the synthesis of nanoscale guests embedded in mesoporous carbon materials.

Acknowledgment. The authors gratefully acknowledge the financial support from the National Fundament Research Project (2002CB613305), the National Natural Science Foundation of China with Contract 20633090 and 20571081, and the Shanghai Nanospecial Project with Contract 0652nm014.

CM0709065